

https://doi.org/10.1070/QEL16944

Ultranarrow-waveguide AlGaAs/GaAs/InGaAs lasers

Yu.K. Bobretsova, D.A. Veselov, A.A. Klimov, L.S. Vavilova,
V.V. Shamakhov, S.O. Slipchenko, N.A. Pikhtin

Abstract. **We have designed, fabricated and studied ultranarrow-waveguide heterostructure lasers emitting in the spectral range 1000–1100 nm. The lasers have been characterised by current–voltage, light–current, far-field intensity distribution and internal optical loss measurements. The ultranarrow-waveguide lasers have been shown to have a threshold current density of ~75 A cm^{-2}, internal quantum efficiency near 100% and internal optical loss near the lasing threshold under 1 cm^{-1}, which corresponds to the level of standard heterostructures. We have demonstrated the possibility of obtaining up to 5 W of output power in continuous mode and up to 30 W in pulsed mode, with a beam convergence (FWHM) of 17.8°. The slope of the internal optical loss as a function of pump current for the ultranarrow-waveguide lasers can be markedly lower than that in lasers with a standard design, but internal quantum efficiency drops to 40% with increasing pump current. The use of barrier layers in ultranarrow-waveguide lasers makes it possible to substantially reduce the drop in internal quantum efficiency.**

Keywords: *absorption coefficient, semiconductor laser, internal optical loss, pulsed pumping, energy barrier, ultranarrow waveguide.*

1. Introduction

A topical issue in designing high-power semiconductor lasers for the spectral range 1000–1100 nm is the ability to improve their output optical characteristics, such as output optical power, efficiency, spatial brightness and spectral brightness. The most efficient lasers are based on a separate-confinement double heterostructure and have a quantum well active region and broadened waveguide. Currently, lasers based on such a configuration have a near 100% internal quantum efficiency and low internal optical loss at their lasing threshold [1], but their light–current (L–I) characteristic undergoes saturation, which prevents further improvement of their output characteristics. There is ample evidence [2–6] that the main cause of the saturation is the rise in internal optical loss with pump current and temperature.

Yu.K. Bobretsova, D.A. Veselov, A.A. Klimov, L.S. Vavilova, V.V. Shamakhov, S.O. Slipchenko, N.A. Pikhtin Ioffe Institute, Russian Academy of Sciences, Politekhnicheskaya ul. 26, 194021 St. Petersburg, Russia;
e-mail: bobretsova@mail.ioffe.ru, nike@hpld.ioffe.ru

Received 27 December 2018
Kvantovaya Elektronika **49** (7) 661–665 (2019)
Translated by O.M. Tsarev

Advances in the technology of semiconductor lasers have made it possible to reduce the internal optical loss due to defects and inhomogeneities in heterostructures, so at present the internal optical loss at the lasing threshold is determined primarily by free-carrier absorption in the active region. Piprek [5] and Wang et al. [6] attributed the observed increase in internal optical loss to the increase in carrier concentration in the waveguide. One possible approach to minimising the internal optical loss and, accordingly, enhancing laser characteristics is to minimise the thickness of the waveguide so that laser light would propagate in the material of the emitters, where carrier concentration varies little. Gradient doping of emitters, successfully used in the case of lasers emitting at 1550 nm, made it possible to considerably raise their maximum power [7].

The objectives of this work were to calculate and fabricate working ultranarrow-waveguide heterostructure lasers emitting at wavelengths in the range 1000–1100 nm, assess the effects of basic parameters, such as the doping profile and waveguide thickness, and energy barrier layers on the laser performance. Below, we present our first results on the fabrication and investigation of AlGaAs/InGaAs/GaAs lasers with an optimised ultranarrow waveguide design.

2. Experimental samples

Lasers were produced using MOVPE-grown separate-confinement double heterostructures with quantum well active regions in the AlGaAs/GaAs/InGaAs solid solution system. The parameters of all the heterostructures grown in this study are presented in Table 1. The reference heterostructure used was structure 1, with a lightly doped waveguide broadened to 3 μm and two InGaAs quantum wells intended for λ = 1040 nm. Structure 2 contained an ultranarrow undoped waveguide 210 nm in thickness and a wave propagation region, including lightly doped parts of the emitters. The total thickness of this region was about 2.4 μm. Structure 3 also included an ultranarrow undoped waveguide, 150 nm in thickness, and energy barriers on the waveguide–emitter interfaces, which were expected to prevent carrier leakage from the waveguide to the emitter. The total thickness of the lightly doped part of the emitters in structure 3 was about 4 μm. Structures 2 and 3 each contained one InGaAs quantum well for a laser wavelength of 1040 nm.

All the lasers were made by a standard deep mesa process and had a 100-μm-wide aperture defined by angle-etched mesas, which suppressed closed-mode formation. The lasers had different cavity lengths and different reflectivities of their mirrors, which were formed by cleaved facets. In standard L–I and spectral measurements, we used lasers with a cavity length

Table 1. Heterostructure designs.

Layer	No., composition, thickness and doping		
	1	2	3
Substrate	GaAs	GaAs	GaAs
Buffer	GaAs maximum, N^+	GaAs maximum, N^+	GaAs maximum, N^+
N-emitter	AlGaAs (10 %) 1.5 μm maximum, N	AlGaAs (15%) 1 μm maximum, N 1.2 μm minimum, n	AlGaAs (15%) 1 μm maximum, N 2 μm minimum, n
Barrier	–	–	AlGaAs (30 %) 300 Å minimum, n
Waveguide	GaAs 1.73 μm minimum, n 0.2 μm undoped	GaAs 1000 Å undoped	GaAs 700 Å undoped
QW	Two 90-A-thick InGaAs QWs	InGaAs 90 Å	InGaAs 90 Å
Waveguide	GaAs 0.2 μm undoped 1 μm minimum, p	GaAs 1000 Å undoped	GaAs 700 Å undoped
Barrier	–	–	AlGaAs (30%) 300 Å minimum, p
P-emitter	AlGaAs (30%) 1 μm maximum, P	AlGaAs (15%) 1.2 μm minimum, p 1 μm maximum, P	AlGaAs (15%) 2 μm minimum, p 1 μm maximum, P
Contact	GaAs 0.3 μm maximum, P^+	GaAs 0.3 μm maximum, P^+	GaAs 0.3 μm maximum, P^+

$L = 3000$ μm and mirror reflectivities of 5% and 95%. The mirrors had dielectric coatings. Laser samples studied by launching probe light had a cavity length of 5100 μm and two antireflection-coated mirrors ($R \leq 5\%$). Laser chips were mounted on copper heatsinks. In absorption coefficient measurements, free access to both cavity mirrors was ensured. To this end, we used a heatsink shorter than the laser sample.

3. Experimental study

Samples having 3-mm-long cavities were studied experimentally in several steps. In the first step, standard cw L–I and current–voltage (I–V) measurements were performed and the divergence angle along the fast axis (normal to the heterostructure layers) was measured at room temperature. In the second step, pulsed (100 ns, 1 kHz) L–I characteristics of the lasers were measured as described elsewhere [8]. The peak power P_{peak} at a particular pump current was then calculated as

$$P_{\text{peak}} = \frac{P_{\text{av}} - P_{\text{d}}}{f\tau}, \qquad (1)$$

where P_{av} and P_{d} are the average and dark powers determined using a bolometer; f is the pulse repetition rate; and τ is the pulse duration (evaluated using oscilloscope traces of laser pulses).

The I–V curves of the lasers allowed us to compare their basic electrical characteristics – cut-in voltage and series resistance – which were evaluated by fitting the portion of the I–V curve between 1 and 2 A with a straight line, whose slope yielded the series resistance and whose intercept on the voltage axis yielded the cut-in voltage. The results are summarised in Table 2.

Table 2. Main parameters of the heterostructures.

Average	Structure 1	Structure 2	Structure 3
R_{d}/mΩ	49	87	208
V_{cut}/V	1.145	1.2	1.25
η_{int} (%)	98	93	95
α_{int}/cm^{-1}	0.71	0.6	0.49
J_{th} ($1/L = 0$)/A cm^{-2}	121	76	78
P_{cw} ($I = 5$ A)/W	4.1	3.6	4.2
P_{pulse} ($I = 50$ A)/W	38	21	25
θ_{FWHM}/deg	19.6	28.5	17.8

The internal optical loss α_{int}, internal quantum efficiency η_{int} and characteristic threshold current density J_{th} ($1/L = 0$) (Table 2) were determined in continuous mode by a standard method, by measuring the L–I characteristics of the lasers with different cavity lengths near their lasing threshold. All the heterostructures under study had a near 100% internal quantum efficiency at their lasing threshold and an internal optical loss under 1 cm^{-1}. The lasers based on heterostructures 2 and 3, with an ultranarrow waveguide, had a characteristic threshold current density of ~75 A cm^{-2}, which corresponds to the level of standard laser structures. Because of the larger number of quantum wells in heterostructure 1, the threshold current density in it was considerably higher.

Figure 1 shows characteristic plots of the optical power against pump current for the laser samples under study in continuous and pulsed modes. In continuous mode at low currents, the heterostructures under study have comparable output powers (Table 2). At currents under 5 A, the best results were obtained for the laser based on heterostructure 3. At higher pump currents, however, the highest power was demonstrated by the lasers with the standard heterostructure (structure 1). The lasers having an ultranarrow waveguide and energy barriers (structure 3) turned out to have higher power than the lasers without them (structure 2).

Figure 2 shows far-field intensity distributions along the fast axis of the lasers studied. The output of all the lasers corresponded to the fundamental mode. The smallest beam divergence (full width at half maximum) was offered by the laser structure 3, with an ultranarrow waveguide and barrier layers. The calculated divergences $\Delta\theta_{\text{FWHM}}$ of the laser heterostructures 1, 2 and 3 (20.3°, 24.6° and 15.5°, respectively) correlate with the present experimental data, but there is a marked error in the case of heterostructures 2 and 3, which have ultranarrow waveguides. To improve calculation accuracy, it is necessary in the future to further develop the optical model of the structure, in particular to more accurately assess the effect of doping on the refractive index and guidance properties of the heterostructure.

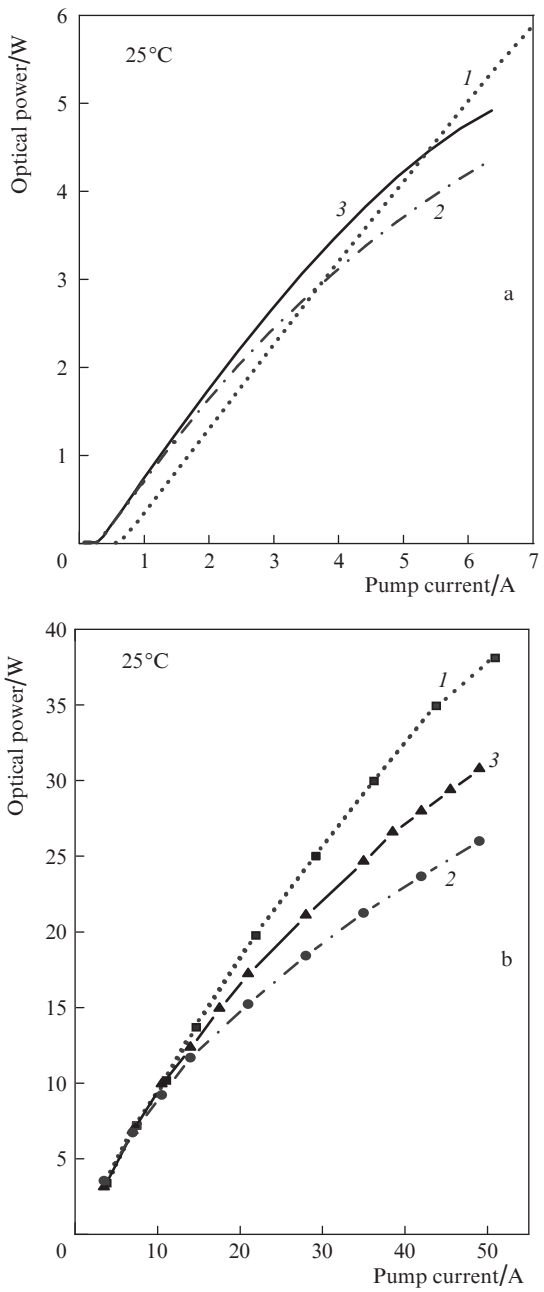

Figure 1. (a) CW and (b) pulsed light–current curves of the lasers based on heterostructures (*1*) 1, (*2*) 2 and (*3*) 3.

The L–I characteristics of the 5100-μm-long laser samples were measured in pulsed mode and, to analyse free-carrier absorption in the waveguide layers of the heterostructures, probe light was launched (the technique used to measure the absorption coefficient was described in greater detail elsewhere [9]).

In our free-carrier absorption measurements, probe light was coupled into the end facet of the laser sample under study in pulsed mode by a lens system. Its wavelength exceeded the laser wavelength in order to eliminate the fundamental absorption and analyse only free-carrier absorption. At the output of the sample, we measured the probe signal power. The change in the absorption coefficient α_{int} was calculated as

$$\Delta\alpha_{\text{int}}(I) = \frac{1}{L}\ln\left(\frac{P_1(I=0)}{P_2(I)}\right), \qquad (2)$$

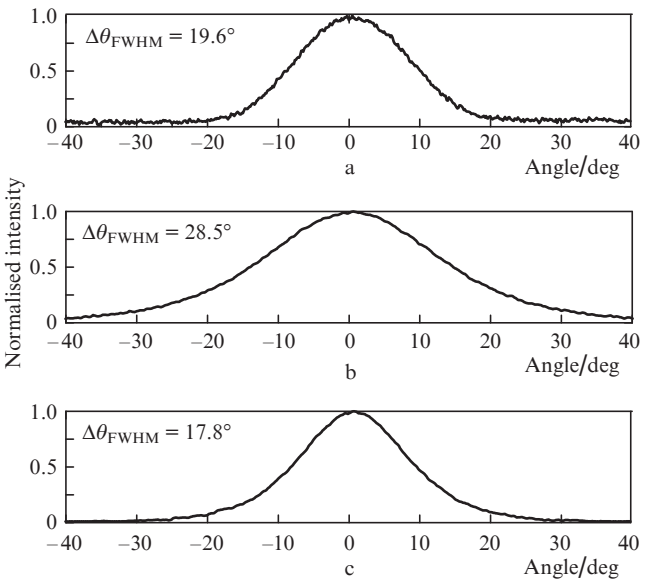

Figure 2. Measured divergence of the lasers based on heterostructures (a) 1, (b) 2 and (c) 3.

where P_1 is the probe signal power at the output of the sample without pumping and P_2 is the probe signal power at the output of the sample at pump current I. P_1 and P_2 were evaluated using oscilloscope traces obtained from a photodetector.

The parameter $\Delta\alpha_{\text{int}}$ is the absorption coefficient change induced in the heterostructure by current I. At zero current, $\Delta\alpha_{\text{int}}$ is zero. From the actual optical absorption in the heterostructure, i.e. from the internal loss in the laser, $\Delta\alpha_{\text{int}}$ differs by a constant term, which is independent of current and arises from scattering by impurities and inhomogeneities in the waveguide. It is convenient to evaluate this term at the lasing threshold from the known measured internal optical loss. The absorption coefficient change measured at the lasing threshold, $\Delta\alpha_{\text{int}}(I_{\text{th}})$, by launching probe light is always smaller than the actual internal optical loss measured by the standard method (I_{th} is the threshold current). The difference between the two values is the sought current-independent, constant term. The sum of the constant term and measured $\Delta\alpha_{\text{int}}(I)$ determines the true dependence of the internal optical loss on pump current.

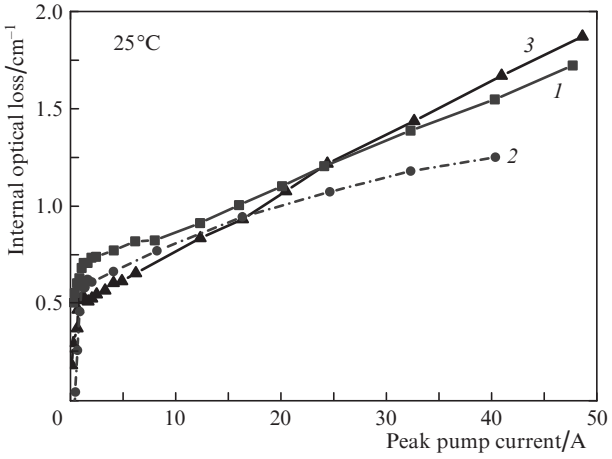

Figure 3. Internal optical loss as a function of pulsed pump current for the lasers based on heterostructures (*1*) 1, (*2*) 2 and (*3*) 3.

Clearly, at $I = I_{th}$ this dependence passes through the optical loss value obtained by standard measurements.

The internal optical loss data obtained are presented in Fig. 3. The lowest internal optical loss at the lasing threshold is offered by heterostructure 3, which has barrier layers and an ultranarrow waveguide (see Table 2). The α_{int} of heterostructures 2 and 3, both having an ultranarrow waveguide, is lower than that of structure 1, which has a broadened waveguide. However, because of the stronger dependence of its internal optical loss on pump current, heterostructure 3 has the highest internal optical loss at currents above 30 A.

4. Discussion of results

The present experimental data (output power and internal optical loss) for the laser samples with a cavity length of 5.1 mm allow their internal quantum efficiency to be estimated as [10]

$$\eta_{int}(I) = \frac{P_{out}(I)}{I - I_{th}} \frac{q}{hv} \frac{\alpha_{out} + \alpha_{int}(I)}{\alpha_{out}}, \quad (3)$$

where P_{out} is the output optical power in pulsed mode; I_{th} is the peak threshold current; I is the pump current of the laser sample under study; α_{out} is the external optical loss; α_{int} is the internal optical loss; q is the electron charge; and hv is the photon energy. The calculation results are presented in Fig. 4. It is seen from these data that the internal quantum efficiency of heterostructure 1 approaches 100% and is essentially independent of the pump current. The quantum efficiency of heterostructure 3, which has barrier layers, falls off to 80% at pump currents below 15 A and is essentially constant at higher pump currents. Heterostructure 2 has the lowest quantum efficiency, which drops to 40% with increasing pump current.

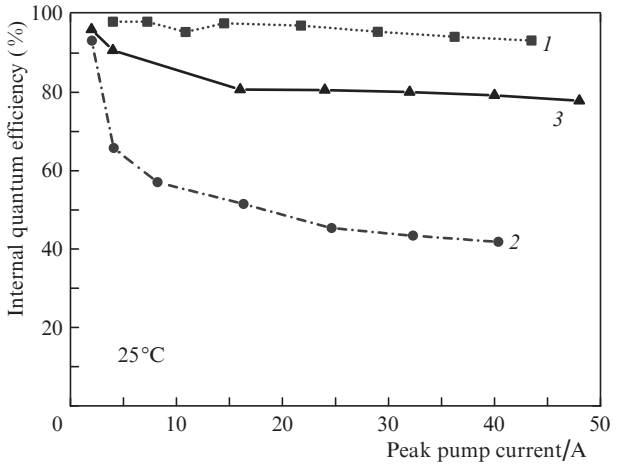

Figure 4. Internal quantum efficiency as a function of pulsed pump current for the lasers based on heterostructures (*1*) 1, (*2*) 2 and (*3*) 3.

On the whole, all the laser heterostructures are comparable in power characteristics, but at the present stage the lasers based on the ultranarrow-waveguide heterostructures are somewhat inferior in power characteristics to the lasers with the standard heterostructure design, which is mainly due to the rapid decrease in internal quantum efficiency with increasing pump current in the former lasers. The addition of barrier layers to the heterostructure design makes it possible to raise the internal quantum efficiency and, accordingly, the output optical power, but leads to a slight increase in the slope of the internal optical loss as a function of current, possibly because of the higher carrier concentration in the waveguide.

For further developing and optimising the ultranarrow-waveguide laser design, it is important to ensure an appropriate doping profile in the emitters. In this study, owing to the large thickness of the lightly doped part we were able to obtain low threshold internal optical losses (at a level of 0.5 cm^{-1}) in heterostructure 3. However, it follows from Table 2 that this impaired its electrical characteristics (series resistance above 200 mΩ). In this context, heterostructure 2 is more optimal: it has a considerably lower series resistance (at a level of 90 mΩ) on account of a slight increase in internal optical loss.

5. Conclusions

We have designed and fabricated ultranarrow-waveguide laser heterostructures emitting in the wavelength range 1000–1100 nm. A number of electrical and optical measurements have been performed on laser samples based on the heterostructures. Ultranarrow-waveguide heterostructure lasers have been shown to have acceptable threshold characteristics: threshold current density at the level of lasers with standard designs, internal quantum efficiency near 100% and internal optical loss under 1 cm^{-1}. The output power obtained, 5 W in continuous mode and 30 W in pulsed mode, does not exceed the level of lasers with a standard, broad waveguide. Nevertheless, the ultranarrow-waveguide heterostructure design offers considerable room for performance optimisation by varying the doping profile and waveguide thickness and utilising energy barrier layers. These latter have been shown to help maintain a high internal quantum efficiency (up to 80%) as the pump current increases, whereas without barriers it drops to 40%. In the ultranarrow-waveguide heterostructures, the internal optical loss also rises with pump current, but its gradient may be lower than that in heterostructures with standard designs.

Further research in this area should be directed towards a search for and optimisation of heterostructure designs, especially the emitter doping profile and waveguide thickness.

Acknowledgements. This work was supported by the Russian Foundation for Basic Research (Project No. 18-32-00151).

References

1. Pikhtin N.A., Slipchenko S.O., Vinokurov D.A., Khomylev M.A., Tarasov I.S. *Proc. OSA/ASSP* (Vienna, 2005) p. WC3.
2. Ryvkin B.S., Avrutin E.A. *Electron. Lett.*, **42** (22), 1283 (2006).
3. Pikhtin N.A., Slipchenko S.O., Sokolova Z.N., Tarasov I.S. *Semiconductors*, **38**, 360 (2004) [*Fiz. Tekh. Poluprovodn.*, **38** (3), 347 (2004)].
4. Sokolova Z.N., Veselov D.A., Pikhtin N.A., Tarasov I.S., Asryan L.V. *Semiconductors*, **51**, 959 (2017) [*Fiz. Tekh. Poluprovodn.*, **51** (7), 998 (2017)].
5. Piprek J. *IEEE Photonics Technol. Lett.*, **30** (10), 963 (2018).
6. Wang X., Crump P., Wenzel H., Liero A., Hoffmann T., Pietrzak A., Schultz C.M., Klehr A., Ginolas A., Einfeldt S., Bugge F., Erbert G., Trankle G. *IEEE J. Quantum Electron.*, **46**, (5) 658 (2010).

7. Marmalyuk A.A., Ryaboshtan Yu.L., Gorlachuk P.V., Ladugin M.A., Padalitsa A.A., Slipchenko S.O., Lyutetskiy A.V., Veselov D.A., Pikhtin N.A. *Quantum Electron*., **47** (3), 272 (2017) [*Kvantovaya Elektron.*, **47** (3), 272 (2017)].
8. Veselov D.A., Kapitonov V.A., Pikhtin N.A., Lyutetskiy A.V., Nikolaev D.N., Slipchenko S.O., Sokolova Z.N., Shamakhov V.V., Shashkin I.S., Tarasov I.S. *Quantum Electron*., **44** (11), 993 (2014) [*Kvantovaya Elektron.*, **44** (11), 993 (2014)].
9. Veselov D.A., Pikhtin N.A., Lyutetskiy A.V., Nikolaev D.N., Slipchenko S.O., Sokolova Z.N., Shamakhov V.V., Shashkin I.S., Voronkova N.V., Tarasov I.S. *Quantum Electron*., **45** (7), 597 (2015) [*Kvantovaya Elektron*., **45** (7), 597 (2015)].
10. Coldren L.A., Corzine S.W., Masanovic M.L. *Diode Lasers and Photonic Integrated Circuits* (New Jersey: John Wiley & Sons, 2012).